Hindawi
Shock and Vibration
Volume 2021, Article ID 5522887, 12 pages
https://doi.org/10.1155/2021/5522887

Research Article

Fault Diagnosis of Subway Traction Motor Bearing Based on Information Fusion under Variable Working Conditions

Yanwei Xu,[1,2] **Weiwei Cai**,[1] **and Tancheng Xie**[1,2]

[1]*School of Mechatronics Engineering, Henan University of Science and Technology, Luoyang 471003, China*
[2]*Intelligent Numerical Control Equipment Engineering Laboratory of Henan Province, Luoyang 471003, China*

Correspondence should be addressed to Yanwei Xu; xuyanweiluoyang@163.com

Received 3 February 2021; Revised 31 March 2021; Accepted 16 April 2021; Published 24 April 2021

Academic Editor: Huaitao Shi

Under the variable working condition, the fault signal of the rolling bearing contains rich characteristic information. In view of the problem that the traditional fault diagnosis method of the rolling bearing depends on the prior knowledge and expert experience too much and the low recognition rate of some faults with the single signal, one method of rolling bearing fault diagnosis based on information fusion under the variable working condition is proposed. Firstly, one test and multi-information acquisition system of the rolling bearing is built. Secondly, the metro traction motor bearing nu216 is selected as the research object, and to prefabricate the defects, the data of acoustic emission and vibration acceleration signals during the test of the bearing is acquired. Then, the original signal is processed and extracted by the wavelet packet decomposition, and the normalized feature information is fused by the convolution neural network. Finally, the two-dimensional convolution neural network model is established to diagnose the bearing fault of the metro traction motor under different conditions. The test results show that the intelligent fault diagnosis method of the subway traction motor bearing based on information fusion under variable working conditions can accurately identify the fault type of the bearing, while the load and speed change. When the neural network training set and the test set cover the same working conditions, the accuracy can reach 100%.

1. Introduction

Operating under the harsh working conditions of high temperature, alternating load, and long-time fatigue causes cracks, pitting corrosion, and other local damage or defects on the inner and outer ring raceways and rolling elements of the metro traction motor bearings, and it can cause abnormal noise and vibration of the traction motor. As a key component of the metro power system, once the traction motor bearing fails, it will affect the smooth running of the subway, abnormal operation, or even damage the equipment which may cause serious economic losses and even casualties. If the incipient and evolving faults of traction motor bearing in operation can be identified accurately, timely, and intelligently, it will be of great significance to the safe operation of subway[1].

Traditional mechanical fault diagnosis is mainly classified by different pattern recognition methods based on extracting shallow fault features through the signal processing and diagnosis experience. For example, Amirat et al. [2] used the overall empirical mode decomposition method to study the fault diagnosis of the wind turbine bearing; Wang et al. [3] studied the intelligent fault diagnosis of support vector machine application. These studies have achieved good diagnosis results, but need to master a lot of signal processing technology and rich engineering practice experience for fault feature extraction [4–6], and less consideration is given to the influence of working conditions on fault diagnosis results. It contains rich fault feature information in the fault signal of the rolling bearing under design conditions. In recent years, many scholars have studied the feature extraction method of rolling bearing fault under the off design condition. For example, Zhao et al. [7] proposed a time-varying nonstationary fault feature extraction method of the rolling bearing based on adaptive generalized demodulation transform; Gao et al. [8]realized rotational

frequency estimation and feature extraction through time-frequency extrusion and resampling order ratio analysis to diagnose bearing fault; Zhou and He [9] proposed a rolling bearing fault intelligent diagnosis model based on independent feature selection and correlation vector machine for variable load conditions. These methods of rolling bearing fault diagnosis under different working conditions have achieved good diagnosis effect, but mainly concentrated in the signal of time-frequency analysis, processing, and feature extraction.

In recent years, artificial intelligence has been widely used in various fields. Many scholars have studied machine learning methods. For example, Han et al. [10] proposed a probability-based prediction method by considering probabilistic feature parameters, to predict the service safety life (SSL) of aeroengine turbine blades effectively. Fei et al. [11] proposed an Enhanced Network Learning Method (ENLM) by introducing Generalized Regression Neural Network (GRNN) and Multipopulation Genetic Algorithm (MPGA) into the Extreme Response Surface Method (ERSM), which improved the modeling accuracy, simulation efficiency, and the reliability of the flexible mechanism, and Fei and Bai [12] proposed the WCFSE FSVM method based on wavelet correlation feature scale entropy. Combining the advantages of the Wavelet Correlation Feature Scale Entropy method and Fuzzy Support Vector Machine method, it can analyze the vibration signal of the aeroengine more accurately and has high generalization ability and antinoise ability. By learning the internal rules and representation levels of sample data, repeatedly nesting feature transformation, and automatically learning the internal characteristics of the data, deep learning can actively mine the representative diagnostic information hidden in massive original data and can directly establish the accurate mapping relationship between the running state and the original data. It largely gets rid of the dependence on the experience of artificial feature design and engineering diagnosis [13]. For example, Lei et al. [14] used deep neural networks and big data to carry out health monitoring of mechanical equipment; Jiang Hongkai [15] and others used deep learning to carry out intelligent diagnosis of aircraft faults. All these studies have achieved good results. The advantages of automatic learning of internal characteristics of data make deep learning successful in the field of rolling bearing fault diagnosis. For example, Li Heng [16] used short-time Fourier transform, Zhang et al. [17] used the multichannel sample construction method, and Chen et al. [18] used the discrete wavelet transform and convolution neural network, respectively, to study rolling bearing fault based on deep learning. All of these methods using the convolution neural network to intelligently diagnose the fault of the rolling bearing have achieved good results, but they are based on the test data collected by Case Western Reserve University.

Information fusion technology is more and more widely used in the field of rolling bearing fault diagnosis. For example, Fei et al. [19] proposed the multifeature entropy distance method for the process character analysis and diagnosis of rolling bearing faults by the integration of four information entropies in time domain, frequency domain, and time-frequency domain and two kinds of signals including vibration signals and acoustic emission signals, and it reveals the rolling bearing operating status more accurately. However, the application of information fusion technology in the field of rolling bearing fault diagnosis has not yet formed a unified specification. To solve the problem of the feature extraction by the time domain, frequency domain or time-frequency domain analysis is too dependent on prior knowledge and expert experience, and it is isolated from the establishment of the model, which results in the restriction of generalization ability for complex classification problems such as bearing fault diagnosis of the metro traction motor. In this paper, the convolution neural network is used to fuse the acoustic emission and vibration information characteristics during the bearing test of the metro traction motor under different working conditions, and the intelligent fault diagnosis method of the metro traction motor bearing based on deep learning and information fusion is studied under variable working conditions.

2. Bearing Test and Information Acquisition System of the Metro Traction Motor

2.1. System Structure. The principle of the rolling bearing test and information acquisition system is shown in Figure 1, which consists of a rolling bearing test bed, test bearing, acoustic emission and vibration sensor, signal amplifier and conditioner, data acquisition card, and computer.

The rolling bearing test platform is jointly developed by Henan University of Science and Technology, Luoyang Bearing Research Institute, and Henan Engineering Laboratory of Intelligent Numerical Control Equipment (it can load 300 kN radial force and 200 kN axial force. The maximum allowable inner diameter of the test bearing is 120 mm); PCI-8 acoustic emission instrument (signal-noise ratio 4.5, the frequency range is 1 kHz–3 MHz, and the maximum sampling frequency is 10 m/s), R50S-TC acoustic emission sensor (the measurement range is 50kHz–700kHz, and the resonant frequency is 500 kHz), LC0151 T acceleration sensor (sensitivity 150 mV/g, range 33G, resolution 40 kHz, resonant frequency 0.0002 g, and frequency range 0.7 Hz–13 kHz), LC0201-5 signal conditioning unit, PCI8510 data acquisition card (speed 500 k/s, 8 channels' synchronous sampling), and NU216 metro traction motor bearing (the inner ring diameter is 80 mm, the outer ring diameter is 140 mm, and the width is 26 mm) jointly build the metro traction motor bearing test and physical information collection system shown in Figure 2.

2.2. Test Bearing and Defect Prefabrication. The test bearing is the NU216 cylindrical roller bearing. Six types of cracks and pitting defects were fabricated on the outer ring, inner ring, and rolling body of the bearing by using the Daqing YLP-MDF-152 3D optical fiber laser marking machine (defect size: crack width of 30 um, pitting diameter of 40 um, and depth of 30% of laser energy). Figure 3 shows the defects of the precast bearing outer ring.

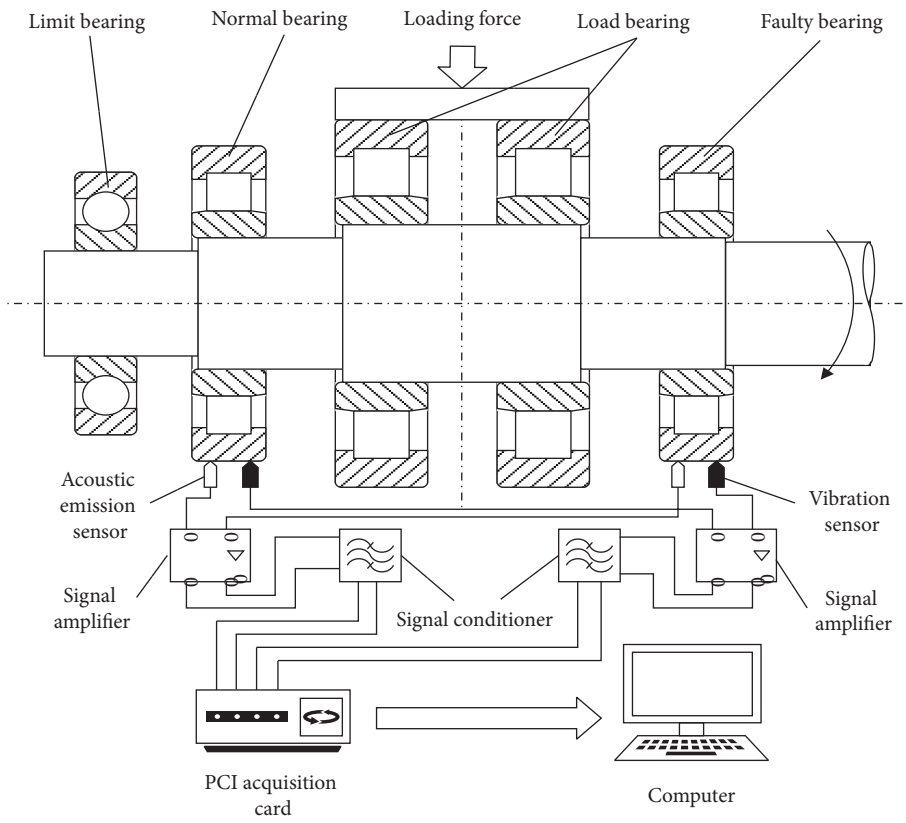

Figure 1: Schematic diagram of the rolling bearing test and information acquisition system.

Figure 2: Bearing test and information collection system of the metro traction motor.

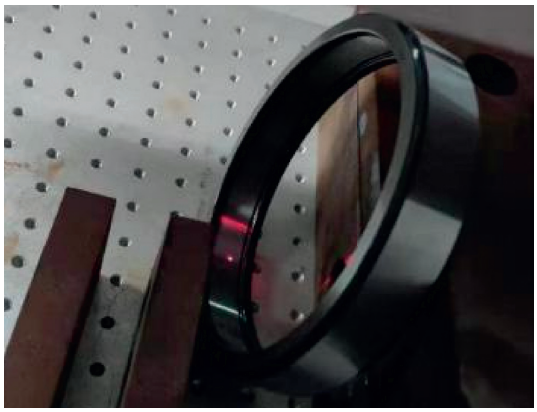

Figure 3: Prefabricated defect on the bearing outer ring.

2.3. Test Parameters and Test Plan. Under actual working conditions, the radial load of the subway traction motor bearing in stable operation is 7 kN, and the speed is 4800 rpm. Due to the limitation of the loading bearing, the maximum speed of the subway traction motor bearing test platform is 2400 rpm. Theoretically, there should be differences in the signal characteristics generated by the various defects of the subway traction motor bearing under the same speed and load. During the operation of subway vehicles, the speed increase, the relative uniform speed, and the deceleration are repeated, and the station interval, passenger flow, and slope are constantly changing, so if using the data under the same speed and load when analyzing the bearing signals of subway traction motors, the effective data will be greatly reduced. And, due to changes in passenger capacity, the signal characteristics of the same location will also change slightly. And, the changes of speed and load may cause subway traction motor bearings with different defectives to produce similar signal characteristics under certain speed and load, which will further affect the diagnosis result. Therefore, three loads and speeds are set to simulate the working conditions of subway traction motor bearings under high speed, medium speed, and low speed and large load, medium load, and low load. According to the actual working conditions of the subway traction motor bearing, 1/4th of the radial load in stable operation is taken as the fluctuating value, and the test is carried out according to the gradient equivalent dynamic load of 5 kN, 7 kN, and 9 kN after rounding. At the same time, the gradient speed was

selected as 800 rpm (low speed), 1600 rpm (medium speed), and 2400 rpm (high speed). The variables in the test are fault type, speed, and load. There are altogether 54 seed tests ($6 \times 3 \times 3 = 54$). The test arrangement is shown in Table 1.

Introduce changes in load and speed to adapt to the diagnosis between samples of known working conditions (speed and load) and samples of unknown working conditions (or between samples of cross-working conditions), and it is expected to realize the diagnosis of adaptive working conditions.

3. Signal Analysis and Feature Selection

3.1. Test Signal Analysis. The vibration signals of six types of bearing under the same working conditions of 2400 rpm and 7 kN are collected, and the frequency distribution diagram is shown in Figure 4.

It can be seen from Figure 4 that there are obvious differences in the frequency band of 5000 Hz–10000 Hz for the bearing of six fault types, and the difference is slight between 0 Hz–5000 Hz and 10000 Hz–25000 Hz.

However, under the actual working conditions, the load and speed will also change due to the change of the subway track gradient, the number of passengers, and so on. The vibration signals of the bearing with outer ring crack under the test conditions of the same speed (2400 rpm) and different loads (5 kN, 7 kN, and 9 kN) are collected, and the frequency distribution diagram is shown in Figure 5; the vibration signals of the bearing with outer ring crack under different speeds (800 rpm, 1600 rpm, and 2400 rpm) and the same load (5 kN) are collected, and the frequency distribution diagram is shown in Figure 6.

It can be seen from Figures 5 and 6 that the influence of speed change on the signal is greater than that of load change; for the same fault bearing, the frequency distribution and frequency amplitude are clearly different under different speeds and loads. From a global point of view, the differences caused by speed and load may make the differences between different types of bearings overlap. The acoustic emission signal is similar to the vibration signal and will not be described in detail.

3.2. Feature Selection. When the bearing fault is small or even weak, due to the low signal-to-noise ratio, the extracted signal features cannot reflect the real situation of the fault. In this case, the frequency range can be predetermined, then the signal is processed by using a filter, and finally the features are extracted. In this paper, there are differences in all kinds of fault types of bearings in the whole frequency band, and the conventional filtering method cannot describe the differences of various fault types of bearings. Since wavelet packet decomposition [20] is an analysis method with good local characteristics in both the time domain and frequency domain, the 8-level wavelet packet decomposition method is used to divide the original signal into 256 frequency bands in this paper; then, according to the frequency distribution obtained from the test, the root mean square value, kurtosis value, and margin value are extracted as the initial eigenvalues, and the initial eigenvector is formed after combination. The calculation formulas of root mean square (RMS), kurtosis (KR), and margin (c) are as follows:

Table 1: Test schedule.

Speed (r/min)	Inner ring (kN)		Outer ring (kN)		Rolling element (kN)	
	Crack	Pitting	Crack	Crack	Pitting	Crack
800	5	5	5	5	5	5
800	7	7	7	7	7	7
800	9	9	9	9	9	9
1600	5	5	5	5	5	5
1600	7	7	7	7	7	7
1600	9	9	9	9	9	9
2400	5	5	5	5	5	5
2400	7	7	7	7	7	7
2400	9	9	9	9	9	9

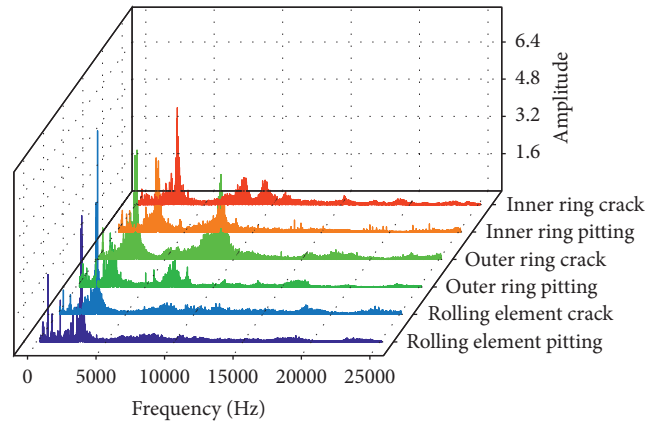

Figure 4: Frequency distribution of bearing vibration signals of six fault types under the same working condition.

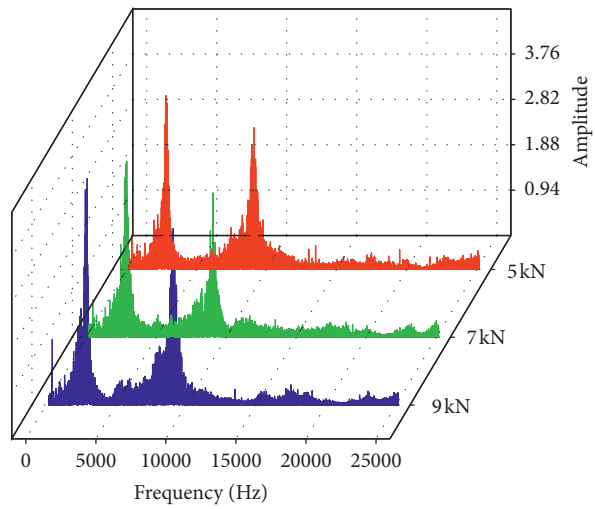

Figure 5: Frequency distribution of the vibration signal of outer ring fault under the same speed and different loads.

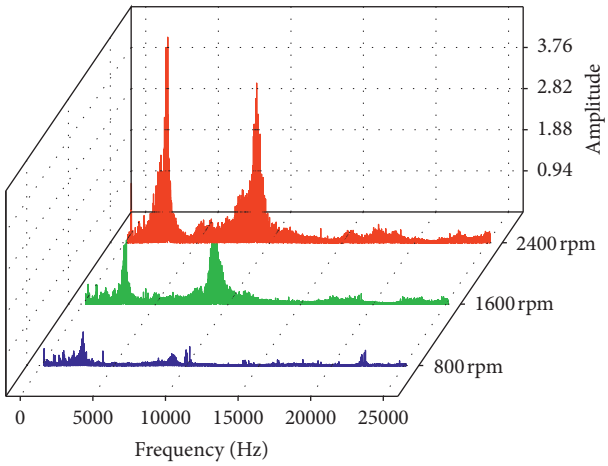

Figure 6: Frequency distribution of the vibration signal of outer ring fault under the same load and different speeds.

$$\text{Rms} = \sqrt{\frac{1}{N}\sum_{i=1}^{N} x_i^2},$$

$$K_r = \frac{N\sum_{i=1}^{N} x_i^4}{\text{Peak}^4} = \frac{N\sum_{i=1}^{N} x_i^4}{\left[(1/n)\sum_{j=1}^{N} x_{pj}\right]^4}, \tag{1}$$

$$C = \frac{x_{\text{Rms}}}{\overline{x}} = \frac{\sqrt{(1/N)\sum_{i=1}^{N} x_i^N}}{(1/N)\sum_{i=1}^{n} x_i}.$$

Considering the influence of the original signal, there are 1542 elements in the initial eigenvector Z^m ($(256 + 1) * 3 * 2 = 1542$). After normalization, the initial eigenvector Z^m is obtained.

4. Information Fusion

Information fusion is an information processing process in which the measurement information of several sensors acquired according to the time sequence is automatically analyzed and comprehensively processed by the computer under certain criteria, to complete decision-making and estimation tasks. Compared with single-information source signal processing technology, information fusion technology is more reliable and effective. According to the level of fusion, it can be divided into data-level fusion, feature-level fusion, and decision-level fusion. Among them, feature-level fusion is to preprocess the information, extract the features, and then fuse the feature information, which not only retains the important features of the input information but also greatly reduces the amount of computation. Compared with data layer fusion, although the amount of data in the feature layer is not as much as that in the data layer, the amount of data in the feature layer is still large. The convolution neural network can extract the features of the diagnosis objects adaptively. In this paper, a convolutional neural network is used to fuse information in the feature layer.

Convolution neural network can process the original signal directly. However, the dimensions of the signals collected by vibration sensors and acoustic emission sensors are different, and even the magnitude of features extracted from single sensor signals is not the same in different scales. Therefore, the original signals must be preprocessed strictly before information fusion.

In this paper, wavelet packet decomposition is used to process the original signal, and then, the multistage signal with different frequency information is obtained. Then, the multistage signal is processed, and the original features are quantized to obtain the original features, and the original features are combined to form the feature vector. Let the eigenvector of the signal collected by a single sensor be Z_i ($i \in 1, 2, \ldots$). The eigenvector of multisensor synthesis is $\mathbf{A}$; the relationship between $\mathbf{A}$ and Z_i and the elements in $\mathbf{A}$ are shown in the following formulas:

$$\mathbf{A} = \left[\mathbf{z}_1, \mathbf{z}_2, \ldots, \mathbf{z}_m\right]^T, \tag{2}$$

$$\mathbf{A} = \begin{pmatrix} a_{11} & \cdots & a_{1n} \\ \vdots & \ddots & \vdots \\ a_{m1} & \cdots & a_{mn} \end{pmatrix}, \tag{3}$$

where n is the number of extracted eigenvalues and M is the number of samples.

The dimension of each element in the eigenvector matrix A is still not uniform, which does not conform to the data format processed by the neural network. Because the neural network focuses on capturing the differences between different types of data and the feature vectors only compare elements in the same position, it is necessary to convert the values of each element from an absolute value to a relative value to meet the requirements of the neural network. Let the set of elements in each column be N_j, and the characteristic matrix after normalized transformation is $\mathbf{B}$. The relationship between N_j and $\mathbf{B}$ is shown in formula (4); if the element in $\mathbf{B}$ is b_{ij}, then the transformation relationship is formula (5):

$$\mathbf{A} = (\mathbf{N}_1, \mathbf{N}_2, \ldots, \mathbf{N}_n), \tag{4}$$

$$b_{\text{ij}} = \frac{a_{\text{ij}}}{\min\left(N_j\right)} - 1. \tag{5}$$

In this case, the maximum value F_j in b_{ij} is shown in the following formula:

$$F_j = \frac{\max\left(N_j\right)}{\min\left(N_j\right)} - 1. \tag{6}$$

Therefore, the numerical range of elements in N_j is $(0, F_j - 1)$. The elements in the transformed characteristic matrix $\mathbf{B}$ are as follows:

$$\mathbf{B} = \begin{pmatrix} b_{11} & \cdots & b_{1n} \\ \vdots & \ddots & \vdots \\ b_{m1} & \cdots & b_{mn} \end{pmatrix}. \tag{7}$$

The transformed eigenvalues are all greater than 0, and the maximum value F_j of each column element is still uncertain. It is necessary to normalize b_{ij} of elements in **B** before inputting the neural network. The traditional normalization method usually converts all data into a specific interval through linear or nonlinear processing. The premise of this method is that the numerical range of the data is known, so it can be compared with each other, so it can be globally normalized. However, the data in this article is collected by two sensors and consists of three eigenvalue arrangements. The value range of each column of data N_j is $(0, F_j - 1]$, where the value of F_j is not certain, that is, the value ranges between different columns of data are different, so they cannot be compared with each other. The data processed column by column can still reflect the difference between different rows of data. Therefore, a column-by-column normalization method is used to further convert the eigenvalues to the same numerical range for use by the neural network. The difference between the column-by-column normalization method used in this article and the traditional normalization method is shown in Figure 7.

Let each column element in the characteristic matrix **B** be $M_{j,}$ and the normalized signal is c_{ij}, then the conversion relationship between b_{ij} and c_{ij} is shown in the following formula:

$$c_{ij} = \frac{b_{ij} - \min\left(M_j\right)}{\max\left(M_j\right) - \min\left(M_j\right)}. \tag{8}$$

5. Convolution Neural Network

Convolution neural network is a kind of feedforward neural network which contains convolution calculation and has deep structure. It adopts an unsupervised or semisupervised learning mode and can classify the input information according to its hierarchical structure. It can automatically and accurately identify the common features of the same kind of signals and the difference features of different kinds of signals, to obtain the high-level abstraction of image data. It overcomes the shortcomings of traditional feature extraction, such as over dependence on prior knowledge and expert experience, low precision, and difficulty in generalization.

Figure 8 shows the structure of the convolution neural network [21, 22], including the input layer, convolution layer, pooling layer, full connection layer, and output layer. Convolution layer, pooling layer, and full connection layer constitute the hidden layer. The convolution layer is the feature extraction layer, which uses local links and weight sharing, and uses multiple convolution kernels to extract features from data. In this paper, there are 1542 elements in the feature vector Z^m obtained from the data feature fusion of the two sensors. Because the two-dimensional convolution neural network is used, the elements in Z^m need to be supplemented by 0 operations and then converted into a 40×40 matrix as the input of the two-dimensional convolutional neural network. The convolution layer contains several convolution kernels with the size of 3×3. The moving step size of the convolution kernel is 1, and each convolution kernel element corresponds to a weight matrix. Each neuron in the convolution layer is connected to several neurons close to the region in the upper layer. The size of the region is the size of the convolution kernel. The main function of the convolution layer is to extract the features of the input data.

The convolution layer can be described as a mathematical function. Let the input of the convolution layer be

$$\mathbf{z}^{(l+1)} = w^{(l)} + x^{(l)} + b^{(l)}, \tag{9}$$

where $x^{(l)}$ is the output of the previous layer, and the output is

$$x^{(l+1)} = f\left(z^{(1)}\right), \tag{10}$$

where $w^{(l)}$ is the convolution kernel of the l layer, $b^{(l)}$ is the bias, and f is the activation function.

If the classifier is directly followed by the convolution layer, it may lead to overfitting because of the high input dimension. Therefore, it is necessary to add a pooling layer to reduce the dimension. If the definition of the pooling function is lower, it can be expressed as

$$X_k^{l+1} = f\left(w^{l+1} lower\left(R_k\right) + b^{l+1}\right), \tag{11}$$

where w^{l+1} is the weight and b^{l+1} is the offset of the function.

The pool layer selects and filters the feature graph extracted from the convolution layer and replaces the results of a single point in the feature graph with the statistics of its adjacent regions, which can reduce the number of nodes in the final fully connected layer. In this paper, a 2×2 pooling matrix is used to reduce the number of nodes in the final full connection layer, and the moving step is 2.

The convolution layer can extract the features of data, and the output of the whole convolution layer can be regarded as a new data matrix, which contains the feature information of the input data. Therefore, a second convolution layer can be added for deeper feature extraction, and a pooling layer is added between the two convolution layers for data dimension reduction. After passing through the first layer of the convolution layer, the data is reduced from 40×40 to 38×38 and then through a pooling layer. Because the moving step of the pooling matrix of the pooling layer is 2, the data is converted from 38×38 matrix to 19×19 matrix, realizing the data dimension reduction; then, the data enters the second convolution layer, and the data is reduced from 19×19 to 17×17; then, a pooling layer is added, and the pooling matrix is added. The boundary of the pool layer is filled with 0, and the data is reduced from 17×17 to 9×9. After two convolution layers and pooling layer, the feature depth extraction is realized, and the data dimension is greatly reduced.

The full connection layer is the last part of the hidden layer of the convolutional neural network. The output is obtained by the nonlinear combination of the extracted features and only transmits signals to other fully connected layers. The output layer generally uses the "Softmax" classifier, which is very effective in multiclassification. The full

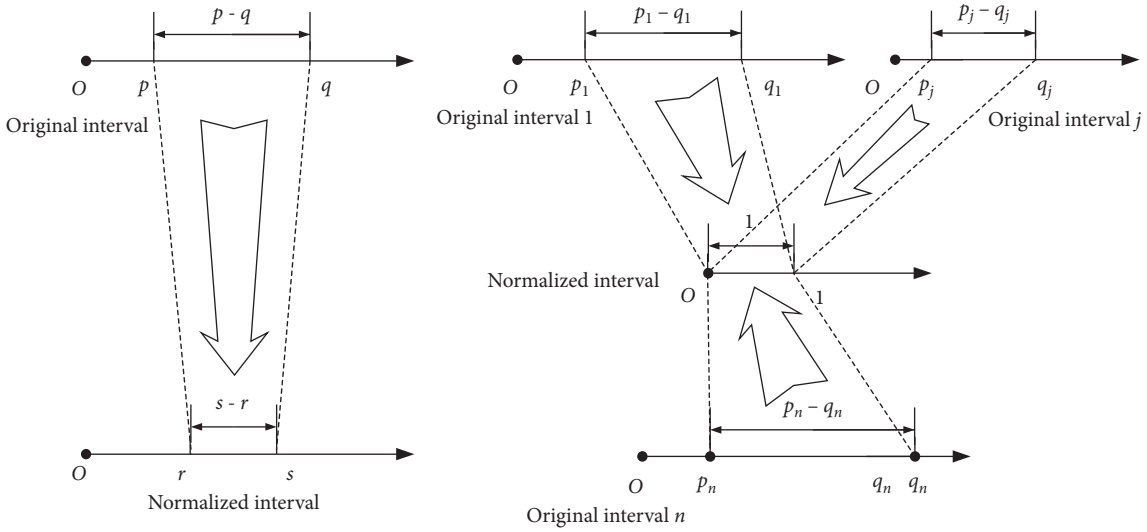

Figure 7: Normalization method.

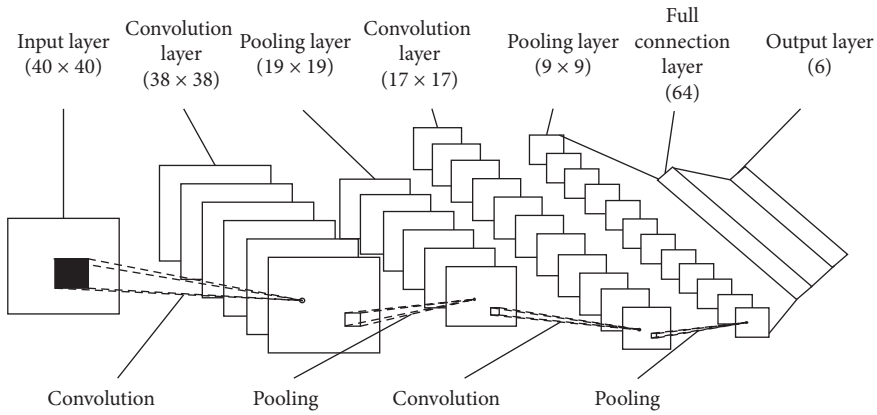

Figure 8: The model of the convolution neural network.

connection layer and the output layer can classify the samples and get the probability distribution of different types of current samples.

The structure parameters of the convolution neural network constructed in this paper include the number of network layers, convolution kernel size, sliding step size, learning rate and training time. According to the number of input layer elements, the convolution layer is 2 layers, the pooling layer is 2 layers, the full connection layer is 1 layer, and the output layer is using the "Softmax" classifier. The convolution kernel is set to 3×3, the sliding step size is set to 1, the learning rate is 0.001, and the activation function is "relu" activation function. If the epochs are set too high, the training time will be greatly prolonged, and even overfitting will be caused. If the epochs are set too low, the recognition accuracy will be affected, so it needs to be tested before determination. In this paper, when the speed is 800 rpm, the data with load of 5 kN and 7 kN are selected as the training set data, and the data with the load of 9 kN is the test set data. The diagnostic error rate and accuracy curve obtained by the preliminary test under single working condition change are shown in Figures 9 and 10 . It can be seen from the figure that when the training times reach 15 times, the ideal state is achieved for the first time, and then, it experiences many ups and downs, so the training is adopted. The accuracy requirement can be met by 25 times.

6. Bearing Fault Diagnosis Method Based on CNN and Information Fusion

To realize the intelligent diagnosis of bearing fault of the metro traction motor under different working conditions and types, firstly, the signals of known working conditions and fault types are used as samples to input the convolutional neural network model for training, and then, the bearing signals of unknown working conditions and fault types are intelligently diagnosed. The process of intelligent fault diagnosis of the metro traction motor bearing based on deep learning and information fusion is shown in Figure 11, which mainly includes the following steps: (1) signal acquisition; (2) signal preprocessing; (3) feature extraction and normalization; (4) information fusion based on the convolutional neural network and training of the deep learning model; (5) testing and diagnosis of test samples; (6) signal

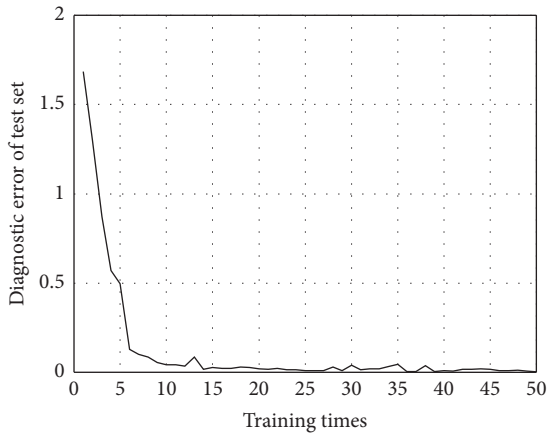

Figure 9: Influence of training time on diagnosis error.

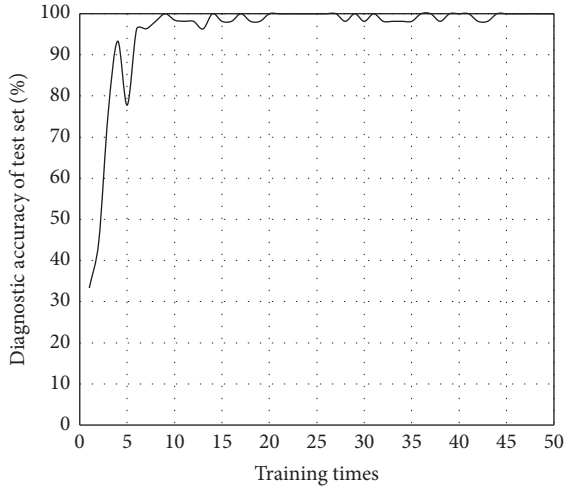

Figure 10: Influence of training time on the accuracy of diagnosis.

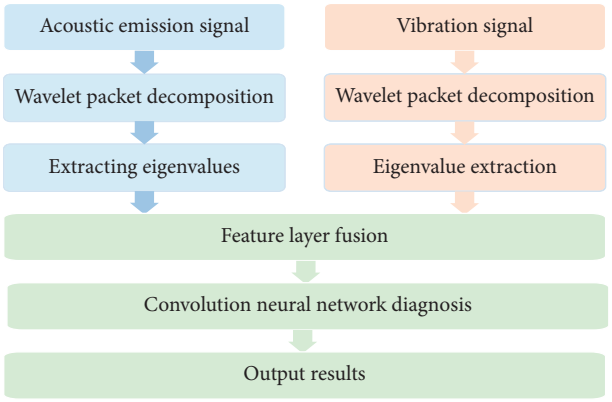

Figure 11: Bearing fault diagnosis process based on deep learning and information fusion.

preprocessing, output the results, and complete the intelligent diagnosis of bearing fault.

In this paper, we use the tensorflow module developed by Google as the basic environment of the convolutional neural network and Python 3.5 as the software programming environment. According to the relationship between the test set and the training set, it is divided into 4 derivation modes, as shown in Figure 12, for intelligent diagnosis.

The main factors affecting the actual operating conditions of subway vehicles are speed and load, and these two factors have a greater impact on the fault signal of the bearing. By changing the speed and the size of the load, the three working conditions of high, low, and medium and mixed working conditions of two factors are simulated to verify the robustness of the diagnostic method under various working conditions. There are 8 basic diagnosis modes shown in Table 2.

In the test, there are 6 types of faulty bearings, four of each type of faulty bearings, and the fault signals were collected under nine working conditions, a total of 216 samples.

6.1. Single Working Condition Fault Diagnosis. Based on the 8 basic diagnosis modes listed in Table 2, the speed and load are controlled, respectively, and the single working condition fault diagnosis is carried out by using the convolution neural network. The diagnosis results are shown in Table 3.

The relationship between the training set and test set in Table 3 covers many situations in the actual test process. Under the condition that the training set and the test set cover the same working conditions, the sample ratio of the training set to the test set is 3 : 1 (Among the 4 samples of each bearing, 3 samples are the training set, and the remaining is the test set), and the rest is 2 : 1 (the training set is 2 working conditions, and the test set is 1 working condition). From the relationship between the test set and the training set, when the test set sample covers the same condition type as the training set sample, the average diagnostic accuracy reaches 100%; when the test set sample is within the training set sample interval, the average diagnostic accuracy reaches 97.92%; when the test set sample is larger than the upper limit of the training set sample, the average diagnostic accuracy rate reaches 94.44%; when the test set sample is smaller than the lower limit of the training set sample, the average diagnostic accuracy reaches 74.31%.

From the diagnosis results of each sensor, the average diagnostic accuracy of using information fusion technology is 91.67%; when using the vibration sensor as the information source, the average diagnostic accuracy is 88.08%; when using the acoustic emission sensor as the information source, the average diagnostic accuracy rate is 74.31%.

In Table 3, the diagnostic accuracy rate of number 23 in Table 3 is low. At this time, the diagnostic accuracy rate of using information fusion technology is less than that of the single information source, which is related to the low diagnostic accuracy rate of the single information source, and the sample size of the test set is smaller than that of the training set.

6.2. Fault Diagnosis of the Composite Working Condition. In the actual operation process, there may also be composite variation conditions, as shown in Table 4. In its diagnosis, the training set and the test set are doped with the changes of

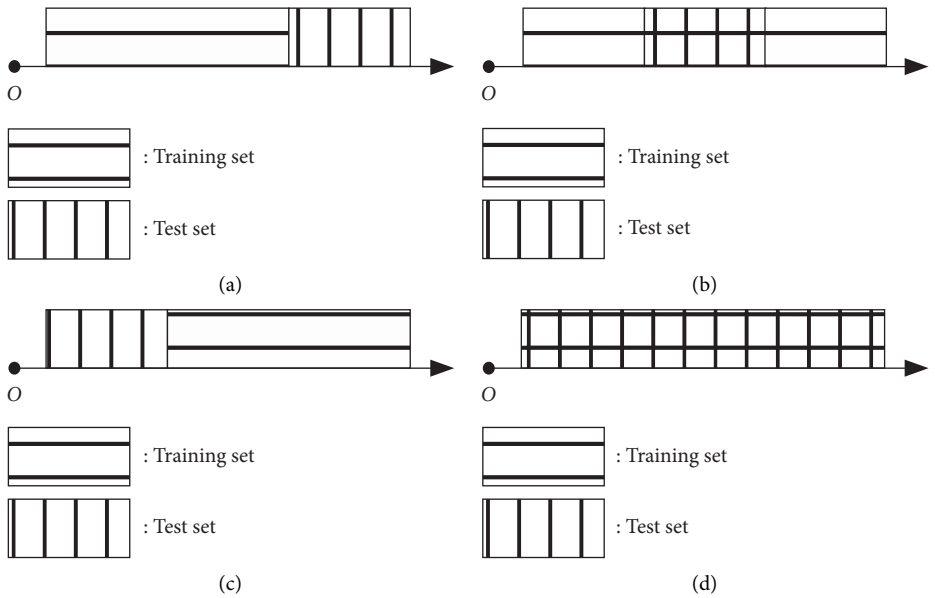

Figure 12: Four models of derivation. (a) The test set sample is larger than the upper limit of the training set sample interval. (b) The test set samples are in the training set sample interval. (c) The test set sample is smaller than the training set sample interval lower limit. (d) The sample interval of the test set is equal to that of the training set.

Table 2: Eight basic diagnostic modes.

No.	Test variable	Training set	Test set
1	Speed (rpm)	800, 1600	2400
2	Speed (rpm)	800, 2400	1600
3	Speed (rpm)	1600, 2400	800
4	Speed (rpm)	800, 1600, 2400	800, 1600, 2400
5	Load (kN)	5, 7	9
6	Load (kN)	5, 9	7
7	Load (kN)	7, 9	5
8	Load (kN)	5, 7, 9	5, 7, 9

load and speed at the same time. The diagnosis results of the training set and test set under two working conditions are also shown in Table 4.

From the working condition relationship between the test set and the training set in Table 4, when the test set sample is within the training set sample interval, the average diagnostic accuracy rate reaches 95.14%; when the test set sample is larger than the upper limit of the training set sample interval, the average diagnostic accuracy rate reaches 90.28%; when the test set sample is smaller than the lower limit of the training set sample interval, the average diagnostic accuracy rate reaches 65.28%.

From the diagnosis results of each sensor, the average value of diagnosis accuracy obtained by using information fusion technology reaches 83.57%; when using the vibration sensor as information source alone, the average diagnostic accuracy reaches 80.79%; when using the acoustic emission sensor as information source alone, the average diagnostic accuracy rate reaches 70.14%. The diagnostic accuracy of No. 3 in Table 4 is low, which is similar to that under the single working condition, and the reason is the same.

6.3. Fault Diagnosis of the Flooding Condition. The training set and test set in Tables 3 and 4 are not generalized to all working conditions. Therefore, the training set and test set contain 54 types of test data at the same time, and the diagnosis results are shown in Figure 12. In the figure, the vertical axis represents the actual bearing fault types, and corresponding to 6 fault types, each fault type contains 9 working conditions, and the measured samples have 54 signals; the horizontal axis represents the probability of the neural network predicting 6 fault types. Therefore, when the diagnosis is correct, the column fault type of the block where the probability value is located is the same as the row fault type.

The output value of the convolution neural network is a probability value (range: 0% ~ 100%). For the unknown signals, there are six output values, namely, a (probability value of the fault being inner ring crack), b (probability value of the fault being inner ring pitting corrosion), c (probability value of the fault being outer ring crack), d (probability value of the fault being outer ring pitting corrosion), e (probability value of the fault being rolling element crack), and f

Table 3: Accuracy rate of single condition fault diagnosis.

No.	Training set speed (rpm)	Training set load (kN)	Test set speed (rpm)	Test set load (kN)	Diagnostic accuracy (%)		
					Acoustic emission	Vibration	Comprehensive
1	800	5, 7	800	9	94.44	95.83	100
2	800	5, 9	800	7	83.33	100	100
3	800	7, 9	800	5	66.67	70.83	91.67
4	800	5, 7, 9	800	5, 7, 9	100	100	100
5	1600	5, 7	1600	9	83.33	100	100
6	1600	5, 9	1600	7	95.83	100	100
7	1600	7, 9	1600	5	95.83	100	100
8	1600	5, 7, 9	1600	5, 7, 9	95.83	100	100
9	2400	5, 7	2400	9	100	100	100
10	2400	5, 9	2400	7	100	100	100
11	2400	7, 9	2400	5	91.67	100	100
12	2400	5, 7, 9	2400	5, 7, 9	100	100	100
13	800, 1600	5	2400	5	45.83	79.17	100
14	800, 2400	5	1600	5	54.17	83.33	100
15	1600, 2400	5	800	5	25.00	41.67	50.00
16	800, 1600, 2400	5	800, 1600, 2400	5	94.44	100	100
17	800, 1600	7	2400	7	54.17	83.33	83.33
18	800, 2400	7	1600	7	62.50	83.33	87.50
19	1600, 2400	7	800	7	33.33	50.00	75.00
20	800, 1600, 2400	7	800, 1600, 2400	7	77.78	100	100.0
21	800, 1600	9	2400	9	37.50	79.17	83.33
22	800, 2400	9	1600	9	75.00	100	100
23	1600, 2400	9	800	9	25	58.33	29.17
24	800, 1600, 2400	9	800, 1600, 2400	9	66.70	88.89	100

Table 4: Accuracy rate of multicondition fault diagnosis.

No.	Training set speed (rpm)	Training set load (kN)	Test set speed (rpm)	Test set load (kN)	Diagnostic accuracy (%)		
					Acoustic emission	Vibration	Comprehensive
1	800, 1600	5, 7, 9	2400	5, 7, 9	73.61	77.78	80.56
2	800, 2400	5, 7, 9	1600	5, 7, 9	69.44	84.72	93.06
3	1600, 2400	5, 7, 9	800	5, 7, 9	25.00	37.50	36.11
4	800, 1600, 2400	5, 7	800, 1600, 2400	9	90.28	97.22	100
5	800, 1600, 2400	5, 9	800, 1600, 2400	7	84.72	97.22	97.22
6	800, 1600, 2400	7, 9	800, 1600, 2400	5	77.78	90.28	94.44

(probability value of the failure is the rolling element pitting corrosion). If a is the maximum value, the final judgment result is of type a; if the value of a is much larger than the other values, the confidence degree of the neural network is higher; if the value of a is not different from other values, the confidence degree of the neural network is low. As can be seen from Figure 13, when the information fusion technology is not used, under the diagnosis mode based on the vibration sensor and acoustic emission sensor, the fault types of inner ring crack and inner ring pitting corrosion are misjudged, and the diagnostic accuracy rate is not 100%, and the overall confidence level is low. After using information fusion technology, not only the diagnostic accuracy rate is improved to 100% but also the confidence level is higher.

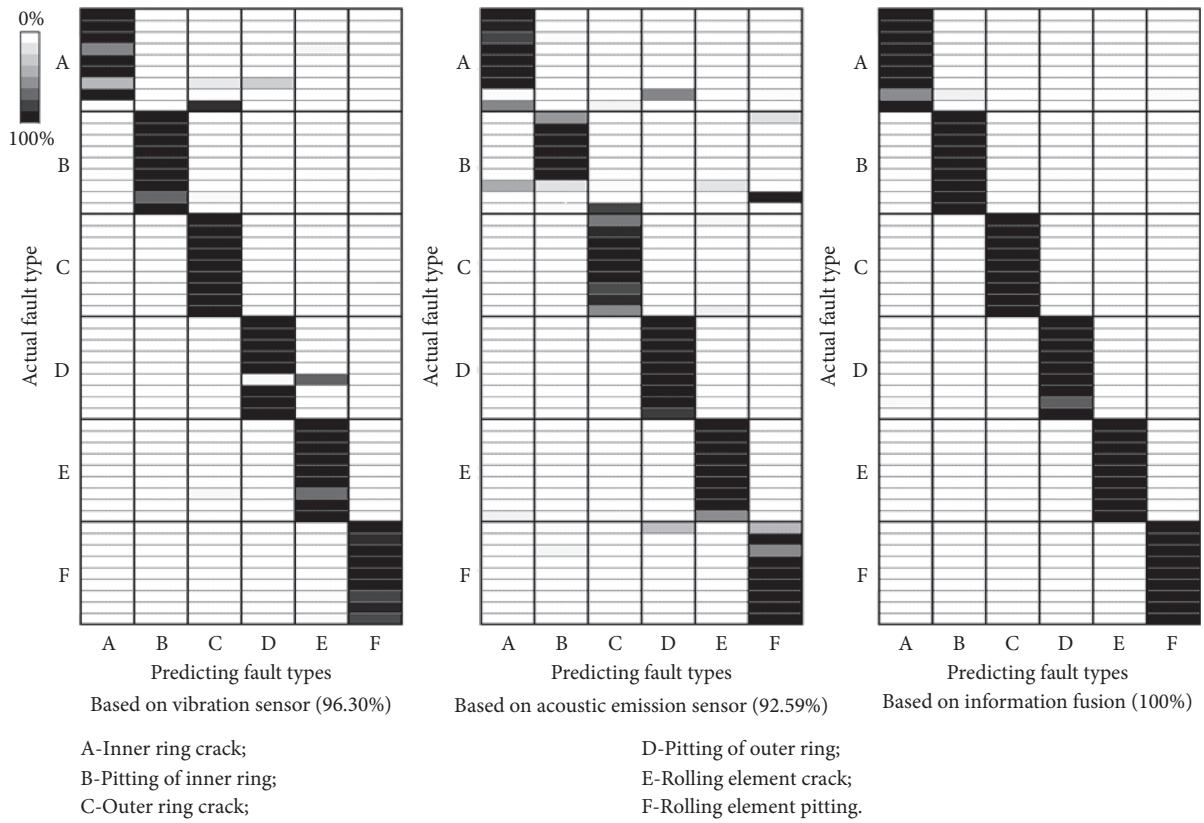

Figure 13: Accuracy rate of general condition fault diagnosis.

In Figure 13, A is inner ring crack, B is pitting of the inner ring, C is outer ring crack, D is pitting of the outer ring, E is rolling element crack, and F is rolling element pitting.

7. Conclusion

Aiming at the problem of time-frequency feature adaptive extraction and intelligent diagnosis in the process of rolling bearing fault diagnosis under variable operating conditions, a method for subway traction motor bearing fault diagnosis based on information fusion under variable operating conditions is proposed.

(1) In this paper, a subway traction motor bearing test and a multi-information data acquisition system are built, and tests under different working conditions are carried out. The wavelet packet decomposition method is used to decompose the original signals of vibration and acoustic emission during the test and extract the features and then fuse the extracted feature information. There are a total of 1542 elements in the feature vector Z^m obtained after the data features of the two sensors are fused. Perform zero-filling operations on the elements in Z^m, add to 1600 elements, and then convert them into a 40×40 matrix as the input of the two-dimensional convolutional neural network. The number of convolutional layers in the convolutional neural network constructed in this paper is 2 layers, the pooling layer is 2 layers, the fully connected layer is 1 layer, and the output layer uses the "Softmax" classifier. The convolution kernel is set to 3×3, the sliding step is set to 1, the learning rate is 0.001, and the activation function is the "relu" activation function.

(2) The results show that ① speed has a great influence on the diagnosis results, but the load has little influence on the diagnosis results; ② increasing the range of various working conditions in the training samples can effectively improve the accuracy rate; ③ when the training sample conditions cover the working conditions of the tested samples, the diagnostic accuracy rate can reach 100%.

(3) This article only considers the faults of three parts of the bearing of the subway traction motor. The bearing cage faults, wear, deformation, and other faults can be studied later.

(4) In this paper, a platform built in the laboratory is used to carry out the research. It is necessary to add devices that can apply vibration loads and shock loads to be closer to subway operating conditions.

Data Availability

The data used to support the findings of this study are included within this article.

Conflicts of Interest

The authors declare that they have no conflicts of interest.

Acknowledgments

The authors are grateful for the financial support of the National Natural Science Foundation of China (51305127) and Scientific Research Key Project Fund of the Education Department Henan Province of China (21B460004).

References

[1] W. He, *Research on Periodic Group-Sparse Feature Extraction and its Applications to Machinery Fault Diagnosis*, Xian Jiaotong University, Xian, China, 2016.

[2] Y. Amirat, V. Choqueuse, and M. Benbouzid, "EEMD-based wind turbine bearing failure detection using the generator stator current homopolar component," *Mechanical Systems & Signal Processing*, vol. 41, no. 1-2, pp. 667–678, 2013.

[3] B. Wang, X. Zhang, F. Aoxiao et al., "Opyimization of support vector machine and its application in intelligent fault diagnosis," *Journal of Vibration, Measurement & Diagnosis*, vol. 37, no. 3, pp. 547–552, 2017.

[4] H. Talhaoui, A. Menacer, A. Kessal, and R. Kechida, "Fast fourier and discrete wavelet transforms applied to sensorless vector control induction motor for rotor bar faults diagnosis," *Isa Transactions*, vol. 53, no. 5, pp. 1639–1649, 2014.

[5] G. Georgoulas, T. Loutas, C. D. Stylios et al., "Bearing fault detection based on hybrid ensemble detector and empirical mode decomposition," *Mechanical Systems & Signal Processing*, vol. 41, no. 1-2, pp. 510–525, 2013.

[6] H. H. Bafroui and A. Ohadi, "Application of wavelet energy and Shannon entropy for feature extraction in gearbox fault detection under varying speed conditions," *Neurocomputing*, vol. 133, no. 8, pp. 437–445, 2014.

[7] D. Zhao, T. Wang, and F. Chu, "Adaptive generalized demodulation transform based rolling bearing time-varying nonstationary fault feature extraction," *Journal of Mechanical Engineering*, vol. 56, no. 3, pp. 80–87, 2020.

[8] G. Gao, W. Huang, L. Ning et al., "Fault detection method for varying rotating speed bearings based on timefrequency squeeze and order analysis," *Journal of Vibration and Shock*, vol. 39, no. 3, pp. 205–210, 226, 2020.

[9] Y. Zhou and C. He, "Bearing fault diagnsis under varying load conditions based on individual feature selection and relevance vector machine," *Journal of Vibration and Shock*, vol. 31, no. 3, pp. 157–161, 2012.

[10] L. Han, C. Cao, T. Guo et al., "Probability-based service safety life prediction approach of raw and treated turbine blades regarding combined cycle fatigue," *Aerospace Science and Technology*, vol. 110, Article ID 106513, 2021.

[11] C. W. Fei, L. Huan, H. T. Liu et al., "Enhanced network learning model with intelligent operator for the motion reliability evaluation of flexible mechanism," *Aerospace Science and Technology*, vol. 107, Article ID 106342, 2020.

[12] C.-W. Fei and G.-C. Bai, "Wavelet correlation feature scale entropy and fuzzy support vector machine approach for aeroengine whole-body vibration fault diagnosis," *Shock and Vibration*, vol. 20, no. 2, pp. 341–349, 2013.

[13] H. Ren, J. Qu, C. Yi et al., "Deep learning for fault diagnosis: the state of the art and challenge," *Journal of Control and Decision*, vol. 32, no. 8, pp. 1345–1358, 2017.

[14] Y. Lei, F. Jia, X. Zhou et al., "A deep learning-based method for machinery health monitoring with big data," *Journal of Mechanical Engineering*, vol. 51, no. 21, pp. 49–56, 2015.

[15] H. Jiang, H. Shao, and X. Li, "Deep learning theory with application in intelligent fault diagnosis of aircraft," *Journal of Mechanical Engineering*, vol. 55, no. 7, pp. 27–34, 2019.

[16] H. Li, Q. Zhang, X. Qin et al., "Fault diagnosis method for rolling bearings based on short-time Fourier transform and convolution neural network," *Journal of Vibration and Shock*, vol. 37, no. 19, pp. 132–139, 2018.

[17] H. Zhang, Y. Qi, B. Zhao et al., "A bearing fault diagnosis method based on multi-channel sample and deep convolutional neural network," *Journal of Xi'an Jiaotong University*, vol. 54, no. 8, pp. y2–y10, 2020.

[18] R. Chen, X. Huang, L. Yang et al., "Rolling bearing fault identification based on convolution neural network," *Journal of Vibration Engineering*, vol. 31, no. 5, pp. 161–169, 2018.

[19] C.-W. Fei, Y.-S. Choy, G.-C. Bai, and W.-Z. Tang, "Multi-feature entropy distance approach with vibration and acoustic emission signals for process feature recognition of rolling element bearing faults," *Structural Health Monitoring*, vol. 17, no. 2, pp. 156–168, 2018.

[20] C. Rajeswari, B. Sathiyabhama, S. Devendiran, and K. Manivannan, "bearing fault diagnosis using wavelet packet transform, hybrid PSO and support vector machine," *Procedia Engineering*, vol. 97, pp. 1772–1783, 2014.

[21] R. Zhao, R. Yan, Z. Chen, K. Mao, P. Wang, and R. X. Gao, "Deep learning and its applications to machine health monitoring," *Mechanical Systems and Signal Processing*, vol. 115, pp. 213–237, 2019.

[22] S. Khan and T. Yairi, "A review on the application of deep learning in system health management," *Mechanical Systems and Signal Processing*, vol. 107, pp. 241–265, 2018.